

Enhancing mechanical strength of carbon fiber-epoxy interface through electrowetting of fiber surface

Xiaoming Chen^{a,1}, Kaiqiang Wen^{a,1}, Chunjiang Wang^a, Siyi Cheng^a, Shuo Wang^a, Hechuan Ma^a, Hongmiao Tian^a, Jie Zhang^{b,*}, Xiangming Li^a, Jinyou Shao^{a,**}

^a Micro- and Nanotechnology Research Center, State Key Laboratory for Manufacturing Systems Engineering, Xi'an Jiaotong University, Xi'an, Shaanxi, 710049, China

^b Electronic Materials Research Laboratory, Key Laboratory of the Ministry of Education & International Center for Dielectric Research, School of Electronic Science and Engineering, Xi'an Jiaotong University, Xi'an, 710049, China

ARTICLE INFO

Keywords:

Carbon fiber
Surface morphology
Interfacial strength
Electrohydrodynamic
Electrowetting

ABSTRACT

The interfacial shear strength between carbon fiber and polymer matrices plays a critical role in bulk mechanical performances of carbon fiber-reinforced polymer composites. However, finding simple and effective methods for modulating the interfacial adhesion remains challenging even after over a decade of research and development. Herein, a novel method based on electrically-assisted wetting technique was developed to strengthen the interfacial adhesion between carbon fiber and polymer matrix. The results indicated the polymer completely infiltrated the small grooves on the fiber surface under applied external electric field during the curing process, leading to the formation of conformal contact interface. The interfacial properties were characterized by utilizing the microdroplet debonding and single fiber fragmentation tests. It is found that the as-prepared composites exhibit a maximum increased interfacial shear strength (IFSS) reaching up to 119.69 MPa, a value 81.02% higher than that of the original fiber-based composites. The reinforcement mechanism was ascribed to the improved wettability and mechanical interlock effect induced by the applied electrical stimulus which was supported by dynamic simulation of two-phase flow. In sum, the suggested simple, facile, and environmentally friendly strategy can effectively regulate the interfacial load transfer capacity, thereby suitable for the optimal design of fiber-reinforced composites.

1. Introduction

Fiber-reinforced polymer composite is a type of engineered material with characteristics of lightweight, high-strength, and great durability. Therefore, they are widely utilized in the fields of aerospace, automobile industries, civil infrastructure, among others [1–4]. Carbon fiber (CF) is an important reinforcement material used in advanced composites due to its high mechanical strength [5–8]. The quest for lightweight and high-strength composites demands strong interfacial adhesion between fibers and polymer matrices since the realization of the reinforcing effect of carbon fiber depends on the transfer of adequate load from the polymer to carbon fiber. Thus, carbon fiber-polymer interface should be considered a top priority during the design of advanced composites, where tremendous efforts have so far been made to improve the interfacial shear strength in composites [9,10].

The surface of carbon fiber is relatively nonpolar and contains many defects and micro/nanostructures, such as surface grooves, concave protrusions, nanocracks, and functional groups. These are prone to increase the surface hydrophobicity of the fiber, leading to decreased wettability of liquid polymers on surfaces of carbon fibers and suppressed penetration of polymers into surface micro/nanostructures. These features lead to the formation of weak interfacial bonding between carbon fibers and polymer matrices [11–14]. To resolve this issue, increasing efforts have been devoted to manipulating carbon fiber surface microstructures to improve the interfacial adhesive strength. These strategies could mostly be classified into two groups: “subtractive” and “additive” surface modifications. Subtractive surface modification mainly relies on increasing the roughness and surface polarity of the carbon fiber surface through physical or chemical reactions aiming to regulate the interface properties of the composites. Examples include

* Corresponding author.

** Corresponding author.

E-mail addresses: jzhang12@xjtu.edu.cn (J. Zhang), jyshao@xjtu.edu.cn (J. Shao).

¹ These authors contributed equally to this paper.

electrochemical modification [15,16], gas/liquid phase oxidation [17,18], plasma treatment [19,20], and electropolymerization [21,22]. Although these methods are simple and fast with significant effects, they are still difficult to precisely control the modification process. In addition, they do not only alter the surface properties but may cause damage to the fiber, thereby reducing its strength [18,23]. Additive surface modification, such as surface deposition [24–26] and coupling agent treatment [27,28], is an alternative approach by which high-strength nanomaterials or transition layer materials are uniformly deposited onto carbon fibers surfaces to improve the wettability and mechanical interlocking between the fibers and polymer matrices [29]. This method induces less damage to the carbon fiber but requires high-cost materials and complex processes, thereby not suitable for mass production [30,31]. Thus, exploring alternative techniques with features of simplicity, controllable process, capability of scalable production, and prevented the decrease in fiber strength and chemical pollution is highly desirable to optimize the interface of composites.

In this work, a novel, simple, and high-efficient approach was developed to enhance the interfacial strength of composites without involving any physical and chemical modification of fibers surfaces. The application of an external electric field allowed complete infiltration of the polymer liquid into small grooves present on fiber surface during curing. This overcame the difficulty of insufficient wetting and limited contact area between the fiber and polymer often involved in traditional processes. The IFSS was characterized by the microdroplet debonding and single fiber fragmentation tests, respectively. The measurements revealed that interfacial load transfer capacity is greatly enhanced with the aid of electrical stimulus. Hence, the proposed method can significantly improve the wettability of polymers on fibers and promote the mechanical interlock under the applied electric field, which was well-explained and supported by two-phase flow dynamics simulations under the electrical stimulus. Overall, the suggested simple method for enhancing interfacial load transfer capacity has potential for designing high-performance fiber-reinforced composites.

2. Experimental

2.1. Materials

The carbon fibers used in this study were PAN-based type supplied by Toray Co. under the trade names of T800H, T800S, and T300B. The wetting effects and interfacial mechanical properties of carbon fiber were investigated by using two kinds of fibers: original received fiber (sizing enameled fiber) and desized fiber. To obtain desized fiber, the original received fibers were first washed in acetone at 40 °C under ultrasonic treatment for 24 h, and then rinsed with methanol and deionized (DI) water followed by drying in a vacuum oven for 10 h. Epoxy resin (E51) and polyamide curing agent (651) were provided by Shanghai Macklin Biochemical Co., Ltd. Diamino diphenyl sulfone (DDS) supplied by Suzhou Yinsheng chemical company was used as curing agent. The Al₂O₃ coated carbon fiber was obtained by depositing an ultra-thin Al₂O₃ insulating layer on carbon fiber surface by atomic layer deposition. Trimethyl aluminum (TMA) and deionized water were utilized as Al and O precursor sources, respectively. Nitrogen (N₂) was employed as carrier gas. The thickness of Al₂O₃ insulating nanolayer after 150 deposition cycles was estimated to be 15 nm.

2.2. Electrically-assisted wetting process

The fabrication of fiber-epoxy composites prepared by the electrically-assisted wetting method can briefly be described by several steps. In this process, carbon fiber and copper plates were used as positive and negative electrodes connected to an external source (TREK COR-A-TROL, model 610B). The gap between the two electrodes was set to a distance ranging from 1 to 10 mm. At the start of fabrication, carbon fiber was firstly impregnated by epoxy resin in a liquid resin tank. An

external electric field at voltages from 0 to 10 kV was then applied between the copper plate and fiber during the curing process.

2.3. Characterization

The surface morphologies of carbon fiber and composites cross-section were characterized by scanning electron microscopy (SEM, HITACHI SU8010) operating at an acceleration voltage of 10 kV. The constituent elements on carbon fiber surface were analyzed by energy-dispersive X-ray spectroscopy (EDS). The morphology and roughness of carbon fiber were identified by atomic force microscopy (AFM, INNOVA). The composition and surface functional groups of carbon fibers were investigated by X-ray photoelectron spectroscopy (XPS, Kratos AXIS ultra BLD, UK) with a monochromatic Al K α source ($h\nu = 1486.6$ eV) at the power of 150 W (15 kV × 10 mA). To compensate for surface charging effect, all binding energies were referenced to C1s neutral carbon peak at 284.6 eV. The mechanical properties of single carbon fiber were evaluated by precision tensile microstage (Linkam MFS 350, UK).

To assess IFSS, micro-droplet debonding tests were conducted. To this end, a single fiber was tightened and fixed on the sample holder, and micro-droplets were prepared by dipping the fiber in the resin matrix multiple times. The resin microdroplets were debonded from the fiber by moving the crosshead of interfacial evaluation equipment (MODEL HM410, Japan). Single fiber fragmentation tests were also used to characterize the interfacial properties. The specimens for fragmentation tests were prepared by mounting the single carbon fiber within a dog-bone-shaped polytetrafluoroethylene mold. Next, epoxy resin was poured into the mold and isothermally cured at 180 °C for 3 h followed by gradual cool down to room temperature. The size of single fiber composite specimens was set to 20 × 4 × 3 mm³ ($L \times W \times H$). Home-made tensile testers mounted with polarized optical microscopes were used for the *in-situ* detection of critical lengths and fringe patterns of fiber fragmentation within the epoxy matrix during the tensile loading process.

2.4. Numerical modeling

Three-dimensional finite element (FE) analyses were conducted to provide insights into the carbon fiber-polymer interfacial adhesion mechanism under applied external electric field during solidification of liquid polymer. The model consisted of a patterned surface, a drop of water, and air. The models were implemented in COMSOL MULTIPHYSICS by performing Maxwell and phase field formulation used to express the coupling between the electric field and flow field. The gap between the fiber surface and electrode was fixed to 1.2 μm, volume of the matrix was 0.77 μm³, and groove width and depth on carbon fiber surface was 150 nm. The carbon fiber was positively charged and upper plate was grounded to form an electric field in middle of the fluid. The viscosity coefficient of the polymer was 0.8 Pa·s, its surface tension coefficient constant was 0.03 N/m, its mass density was 980 kg/m³, and the initial contact angle of the polymer on carbon fiber surface was 120°.

3. Results and discussion

3.1. Morphologies and properties of carbon fibers and interface

Two different types of T800-level carbon fibers (T800H and T800S) were selected, which have the similar mechanical properties and different surface structures. Representative SEM and AFM images of surface morphology and structure of desized T800H and T800S carbon fibers are presented in Fig. 1. Desized T800H (DT800H) showed obvious parallel longitudinal grooves on the surface, while desized T800S (DT800S) looked relatively smooth with fewer and shallower grooves (Fig. 1(a) and (d)). The AFM topography images and representative Z-displacement profiles quantitatively comparing the surface

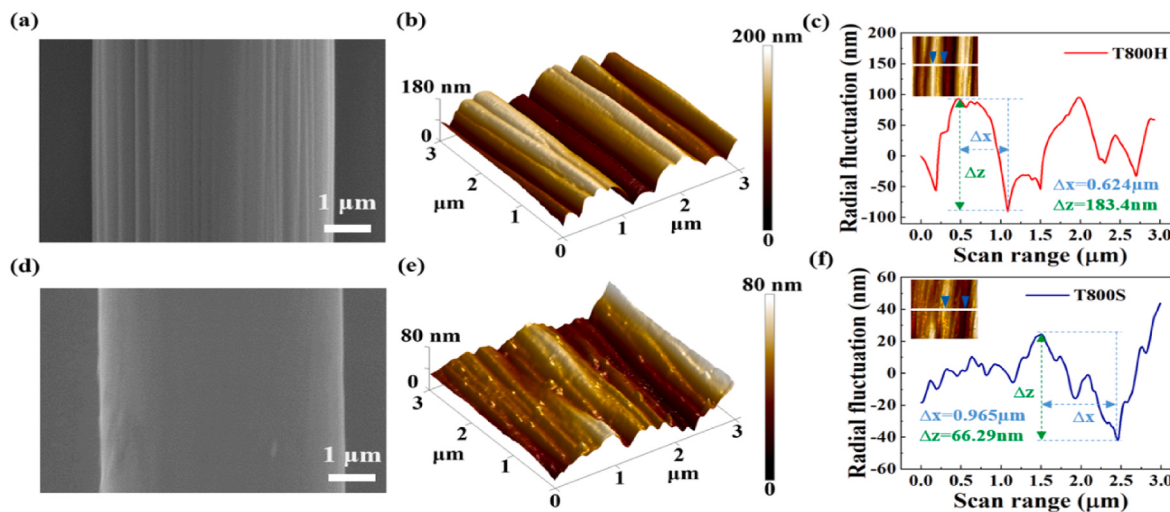


Fig. 1. Surface morphologies of carbon fibers: SEM image (a), AFM topographic (b), and representative Z-displacement profile (c) of desized T800H. SEM image (d), AFM topographic (e), and representative Z-displacement profile (f) of desized T800S.

microstructures of carbon fibers are provided in Fig. 1(b-c) and (e-f). The groove sizes of DT800H looked larger than those of DT800S. The surface roughness (R_a) values of both DT800H and DT800S were estimated to be 45.5 nm and 14.1 nm, respectively. Thus, DT800S fiber surface was smoother, consistent with SEM images. It has been reported the carbon fibers were designed to contain surface grooves for increasing the specific contact area between the fiber and resin, as well as anchoring the fiber into the resin [32]. This would improve the stress transfer capacity and minimize the fiber pull-out during composites fracture. However, enhancing surface grooves on carbon fiber surface induced more additional stress concentration points and cracks, thereby degrading the mechanical properties of carbon fiber. As shown in Table S1 and Fig. S1, T800H displayed slightly lower Young's modulus and tensile strength than T800S.

The interfacial properties of composites might be improved by introducing designed microstructures during the fabrication and surface modification process of fibers [33,34]. However, the interfacial wetting between the fiber and polymer is considered to be a vital but insurmountable issue in realizing the reinforcing effect of carbon fiber. The voids around interfaces between fibers and polymer have always been observed due to the incomplete infiltration of the resin, resulting in nonconformal interface shown in Fig. 2(a). The reason for this can be ascribed to the poor wettability of liquid epoxy resin on carbon fiber

surface during curing process, inducing insufficient infiltration of the resin into surface grooves on carbon fiber and limiting the interfacial contact area [35]. Note that surface microstructures that may promote air entrapment below the liquid resin and resist the penetration of resin fluid could cause Cassie wetting state [36,37]. Therefore, optimizing the surface wetting states from the Cassie state to Wenzel state is extremely important. This can be achieved by forcing the liquid resin to fill the surface microstructures and form “ideal fill” and obtain mechanical interlock interface (Fig. 2(c)), in which additional interfacial friction was provided to restrain the mutual sliding, thereby improving the interfacial strength.

To resolve the issue of incomplete infiltration, an electrically-assisted wetting method was proposed. It has been reported that liquid droplets could fill microcavities/micropores under the applied electrical stimulus [38,39]. Therefore, electrowetting was utilized to promote the wettability of liquid polymer, as well as control the penetration and infiltration of liquid polymer into the carbon fiber surface. A scheme of the process is provided in Fig. 3(a). Carbon fiber and copper plate were used as positive and negative electrodes, respectively. The two electrodes were placed at a certain distance and connected to an external voltage source. At the start of wetting process, carbon fiber was firstly pulled and impregnated with the resin in the liquid tank. Next, the high-voltage power supply was turned on to generate an AC electric voltage with a

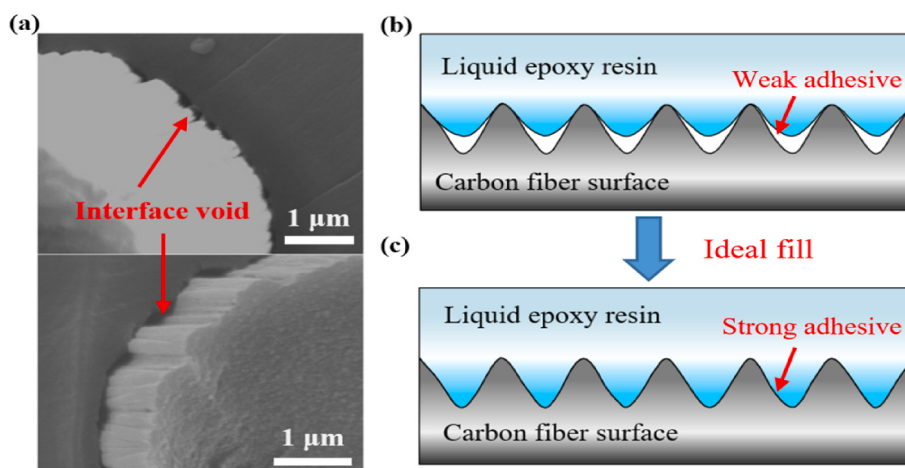


Fig. 2. (a) SEM images of T800H carbon fiber-epoxy interface with obvious voids. (b) Schematic illustrations of fiber-epoxy resin interface shown in (a). (c) Scheme of preferred interface scenario.

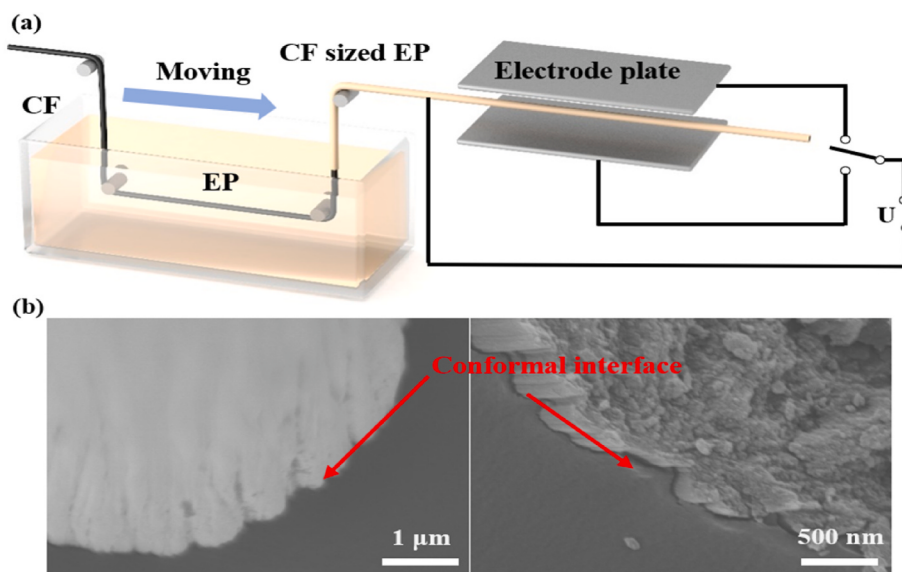


Fig. 3. (a) Schematic illustration of epoxy resin enameled carbon fiber prepared by applied electrically-assisted wetting method. (b) SEM images of cross-sections of nanostructured fiber-epoxy interfaces generated by electrowetting during solidification.

certain field (5 kV/cm) between the two electrodes. It is noted that the electric field intensity is chosen for promoting the noticeable wettability change. During solidification of the epoxy resin on the carbon fiber, the wetting effects of liquid polymer were controlled by electrical stimulus. The interface of the as-prepared composites by the electrically-assisted wetting method is presented in Fig. 3(b). It was observed that the epoxy resin closely stuck to the carbon fiber without any visible voids, suggesting complete filling of the surface grooves by the liquid epoxy, as well as the formation of the conformal interface during the solidification. Thus, wettability of the resin was tailored by the electrical stimulus. It is worth mentioning that anisotropic surface microstructure in the axial and radial direction of carbon fiber may cause inhomogeneous spreading velocity of resin fluid during solidification, however, curing time is sufficiently long to complete the wetting process and reach steady-state. Thus, the full filling of the surface grooves in various directions by the liquid epoxy can be achieved under the electric field. An obvious crack along the interface was observed in the right image of Fig. 3(b) and the crack propagates along carbon fiber surface. Hence, the crack maybe induced during the fracture of composites instead of insufficient filling. It is noted that the electrical stimulus is adopted here for modulating the microscopic wettability instead of macroscopic contact angle. As shown in Fig. S2, the contact angle values increased from 48.2° to 57.1° when applying an electric field up to 5 kV/cm. It is believed that the change of droplet shapes and contact angles were induced by stretching epoxy towards the electrodes under the electric field [38]. But, it is difficult to observe the microscopic wetting state transition through the variation of macroscopic contact angle.

The influence of electrical stimulus on surface microstructure was investigated by XPS to characterize the chemical composition of carbon fibers (Fig. S3). The characterization results of the surface compositions of sized T800H with electrical stimulus (E-T800H), sized T800H without electrical stimulus (T800H), desized T800H with electrical stimulus (E-

DT800H), and desized T800H without electrical stimulus (DT800H) are summarized in Table 1. The percentage of carbon and oxygen atoms in E-T800H and T800H looked nearly the same. The O/C ratios in E-T800H and T800H were estimated to be 20.63% and 20.51%, respectively. It suggests that the electrically-assisted wetting method induced none/few chemical reactions on carbon fiber due to the protection by the sizing agent layer. This did not change the content of elements in fiber. However, the oxygen percentage of E-DT800H slightly increased by 4.17% when compared to DT800H. Also, the O/C ratio in desized T800H significantly rose from 15.81% to 21.68% after the application of the electrical stimulus. The increased oxygen may be linked to the high voltage between both electrodes, which accelerated the oxidation on the carbon fiber surface without sizing the agent protection layer. The detailed chemical analyses of respective C1s spectra in T800H, E-T800H, DT800H, and E-DT800H are presented in Fig. 4. The fitted curve of C1s spectrum can mainly be deconvoluted into three peaks: graphitic carbon (peak I, 284.6 eV), C=O and C=O (peak II, 286.8 eV), and O-C=C (peak III, 288.7 eV) [40]. The profiles of T800H and E-T800H looked nearly identical, where sized carbon fiber consisted of almost 98% C-C, C-O and C=O. As a result, the electrical stimulus had limited effects on the surface chemical composition. In XPS C1s spectrum of E-DT800H (Fig. 4(d)), one significant component peak was observed and attributed to oxygen-containing groups (O-C=O) generated on the fiber surface, suggesting oxidation from -OH and -CHO to -COOH, as well as increase in carboxyl content from 1.72% to 8.59%. However, the oxidation process during the electrical stimulus may not carry on continuously due to the enameling of carbon fiber by the epoxy resin during curing. Table S2 summarized the XPS characterization results of the surface compositions of epoxy resin coated carbon fibers with or without the application of electrical stimulus. The results suggested that the electrical stimulus did not induce chemical reactions on carbon fiber-epoxy surface due to the protection by epoxy layer. Therefore, it is believed

Table 1

Surface element and functional group compositions of the carbon fiber samples before and after applying electrical stimulus.

Samples	Element composition (%)			Functional group composition (%)		
	C1s	O1s	O/C	Peak I C-C	Peak II C=O C=O	Peak III O-C=O
T800H	82.90	17.10	20.63	65.32	33.10	1.58
E-T800H	82.98	17.02	20.51	65.61	32.65	1.74
DT800H	86.35	13.65	15.81	65.11	33.16	1.72
E-DT800H	82.18	17.82	21.68	57.19	34.22	8.59

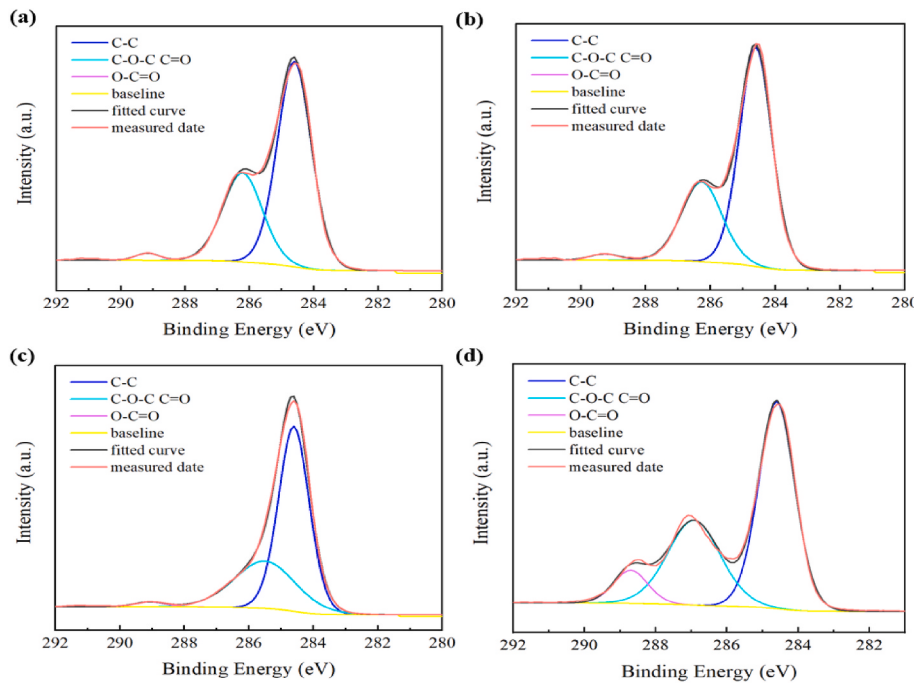


Fig. 4. Comparison of physicochemical properties for sized T800H carbon fiber before (a) and after (b) the application of electrical stimulus. Comparison of physicochemical properties for desized T800H carbon fiber before (c) and after (d) the application of electrical stimulus.

that the electrically-assisted wetting method did not introduce and decompose the functional groups of fibers during composites preparation. In addition, the single fiber tensile strength was tested to detect possible structural damage that may occur during the application of electrical stimulus. The results of single fiber tensile strength were finally analyzed with Weibull statistical model demonstrated that the external electrical stimulus does not cause any discernible change for fiber strength (Fig. S4).

3.2. Interfacial shear strength measurements

To verify the practical promoting effects of electrowetting-induced

mechanical interlock morphologies, the interfacial properties of carbon fiber-epoxy (EP) composites were evaluated by determining the average IFSS via microdroplet debonding testing, as well as the critical length required for efficient stress transfer via single fiber fragmentation testing. A schematic representation of microdroplet test carried out by pulling fiber out of cured epoxy resin droplets is shown in Fig. 5(a). The IFSS value was calculated by assuming uniform stress on the entire interface (Eq. (1)) [41]:

$$\tau_{IFSS} = \frac{F_{MAX}}{\pi d l} \quad (1)$$

where d is the corresponding fiber diameter, F_{MAX} denotes the maximum

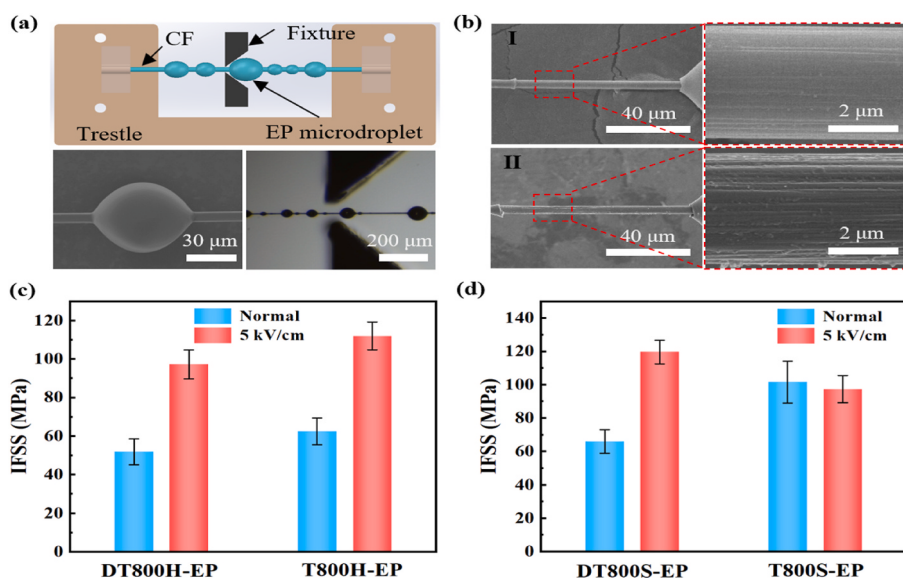


Fig. 5. (a) Schematic diagram of measuring IFSS with micro-droplet test and representing microdroplet for debonding test. (b) Debonded surface of T800H-EP (I) and E-T800H-EP (II) interface. Comparison of calculated average IFSS of (c) T800H-EP interface, and (d) T800S-EP interface before and after the application of electrical stimulus.

load recorded for debonding the microdroplet, and l is the embedded length. The length distribution of the droplets was characterized (Fig. S5). In order to minimize the influence of the embedded length on the IFSS value [10,42], microdroplet lengths ranging from 55 to 65 μm were chosen for IFSS measurement.

Two representative debonded interfaces of T800H- and E-T800H-based composites are illustrated in Fig. 5(b). The surface of T800H looked clean without remaining epoxy after debonding, suggesting the occurrence of apparent brittle debonding at the interface (Fig. 5(b-I)). By contrast, the surface of E-T800H appeared relatively rough with some epoxy residue remaining on the surface, indicating a much stronger interaction between fiber and matrix (Fig. 5(b-II)). The results confirm that employing electrical stimulus enhances fiber-matrix interface strength, as well as changes the debonding morphologies of micro-droplet composites. The quantitative analyses of IFSS of T800H and T800S-based composites are summarized in Fig. 5(c-d). More than 50 micro-droplets were measured for each kind of fiber. The IFSS of desized T800H-epoxy (DT800H-EP) and desized T800S-epoxy (DT800S-EP) composites were estimated to be 51.94 ± 6.83 MPa and 66.12 ± 11.13 MPa, respectively. The difference may be attributed to the intrinsic nature of the rough surface of DT800H and the insufficient interfacial contact in DT800H-EP composites [35]. Under applied electrical stimulus, the IFSS of E-DT800H-epoxy (E-DT800H-EP) and E-DT800S-epoxy (E-DT800S-EP) composites significantly increased to reach 97.26 ± 7.52 MPa and 119.69 ± 7.21 MPa, respectively. This was equivalent to respectively 87.25% and 81.02% increase, ascribed to modulated wettability of the liquid resin by the electrical stimulus, thereby forcing the resin to infiltrate the microstructure like surface grooves on the fiber. This resulted in the formation of mechanical interlocking morphologies between fiber and matrix, as shown in Fig. 3(b). For sized carbon fiber, the T800H-epoxy (T800H-EP) interface demonstrated a very similar trend as that observed for DT800H-EP. However, the IFSS values of T800H-EP and E-T800H-EP were slightly higher than those of interfaces constructed by DT800H and E-DT800H. For example, the IFSS value of T800H-EP was 62.51 ± 6.93 MPa, a value equivalent to 20.35% increase when compared to DT800H-EP. Besides, the IFSS of E-T800H-EP significantly increased by 79.19% when compared to that of T800H-EP composites due to the electrowetting-induced mechanical interlock interface morphology. However, the IFSS value slightly decreased from 101.88 ± 13.46 MPa for T800S-EP interface to 97.26 ± 8.11 for E-T800S-EP, equivalent to 4.53%, indicating electrowetting method generates an increase in mechanical interlock of interface for sized T800S. The reason could be due to two factors. First, the surface grooves and defects on T800S carbon fiber surface were relatively small, as shown in Fig. 1(b). Second, the sizing agent coated on T800S could heal surface microstructure and smooth the surface, leading to slight variations in wetting states of the fiber under the electrical stimulus. To confirm the effectiveness of electrically-assisted wetting method, the polymer matrix was changed from epoxy to photosensitive resin (PR). Fig. S6 presents the IFSS results of four different types of PR-based composites (T800H-PR, E-T800H-PR, DT800H-PR, and E-DT800H-PR). The IFSS values of T800H-PR and DT800H-PR composites showed significant improvement reaching 37.87% and 96.33% after the application of the electrical stimulus, respectively.

Subsequently, the IFSS values of as-prepared composites obtained by the proposed method were compared with previously reported values obtained by various methods. As shown in Table 2, it can be found that the more steps of treatment and the more complex processes, the increase rate of IFSS is higher, which can reach up to 69.67% for T800H-based composites interface prepared by the chemical method with 3 steps [43,44]. Meanwhile, the use of many chemical reagents, such as oxidants can pollute the environment [3,45]. Also, expensive raw materials, such as graphene oxide and carbon nanotubes were employed to improve IFSS, resulting in high-cost processes. By contrast, the electrically-assisted wetting method utilized in this paper was environmentally friendly and low cost, thereby suitable for scalable production.

Table 2

The comparison results show the process and effect of the existing interface modification methods. Among them, C and P represent the chemical and physical modification method used for fiber treatment, respectively; Step represents the process used, such as oxidation, grafting, and deposition.

Carbon fiber	Process	IFSS (MPa)	Max Increase rate (%)
T300	Two steps/C	47.2–84.1	78.2 [3]
T300	Two steps/C	47.9–76.2	59.1 [45]
T300	One step/P	49.8–60.2	20.8 [48]
T700S	One step/P	40.9–47.9	17.1 [49]
T800H	Three steps/C	69–115.7	67.7 [46]
T800H	One step/P	48.85–71.73	46.8 [47]
T800H	Three steps/C	50.26–85.28	69.67 [43]
T800H	Three steps/C	69.8–98.9	41.7 [44]
T800H	One step/P	51.94–97.29	87.25 (This work)
T800S	One step/P	66.12–119.69	81.02 (This work)

Note that carbon fiber reinforced composites based on the electrically-assisted wetting method could achieve higher IFSS than reported results [43,44,46,47].

To validate the great enhancement induced by the mechanical interlock effect instead of chemical bonding, a thin alumina layer with a thickness of 15 nm was deposited on the carbon fiber surface as enamel to insulate and play an inert layer [50]. The chemical stability and electrical insulation characteristics of Al_2O_3 were beneficial to suppress the chemical reactions and prevent the formation of chemical bonding during electrowetting [51,52]. Fig. S7(a-b) shows the elemental characterization obtained by EDS technique. Al_2O_3 deposited onto sized and desized carbon fiber. Fig. S7(c-d) illustrates the IFSS results of composites composed of alumina-coated carbon fiber and epoxy resin. Compared to composites without Al_2O_3 coating (Fig. 5(c-d)), the IFSS values of DT800H-EP, T800H-EP, DT800S-EP, and T800S-EP composites with Al_2O_3 coating on corresponding fibers decreased by 25.26%, 34.22%, 29.45%, and 65.84%, respectively. Such reductions could be ascribed to the poor wettability of alumina and weak van der Waals interfacial interaction. Nevertheless, the electrical stimulus still obviously increased the interfacial mechanical properties (Figs. S7(c-d)). For example, IFSS value displayed a substantial increase from 41.12 ± 4.71 MPa to 65.96 ± 1.83 MPa for sized T800H with Al_2O_3 coating (equivalent to 60.41%), as well as from 38.82 ± 6.09 MPa to 73.11 ± 3.73 MPa for desized T800H with Al_2O_3 coating (equivalent to 88.33%). Although the aluminum oxide film layer on carbon fiber surface weakened the original interface, the electrical stimulus could tailor the wettability of the Al_2O_3 coated fiber and induce mechanical interlock interface, thereby enhancing the mechanical bonding strength.

Overall, the quantitative analyses of microdroplet debonding tests demonstrated the enhancement of IFSS by the electrically-assisted wetting method. To assess the macroscopic performance of single carbon fibers embedded in the matrix and confirm the improvement of interfacial properties by the electrical stimulus, single fiber fragmentation tests of T800H-based composites were conducted by homemade tensile testers, as shown in Fig. S8. IFSS could be calculated based on the micromechanical model of Kelly and Tyson [26]: $\tau_{\text{IFSS}} = \sigma_c d / (2l_c)$. Here, d represents the fiber diameter, l_c is the critical length obtained from average fragment length l_a , l_c is given by $l_c = 4/3l_a$, and σ_c refers to the fiber fracture stress at critical fragment length of fibers. Birefringence images of fragmentation tests carried out with DT800H-EP and DT800H-EP composites under electrical stimulus (named E-DT800H-EP) are shown in Fig. 6(a-b). A noticeable difference was observed in the fragment length between E-DT800H-EP and DT800H-EP composites. The statistics of fragment length in DT800H-EP and E-DT800H-EP composites are provided in Fig. 6(c). The average fragment length l_a of E-DT800H-EP composites (260.18 ± 66.16 μm) was 30.59% shorter than that of DT800H-EP composites (374.83 ± 104.15 μm). According to Kelly and Tyson model [26], the IFSS should be inversely proportional to the fragment length. Hence, E-DT800H-EP composites had a stronger

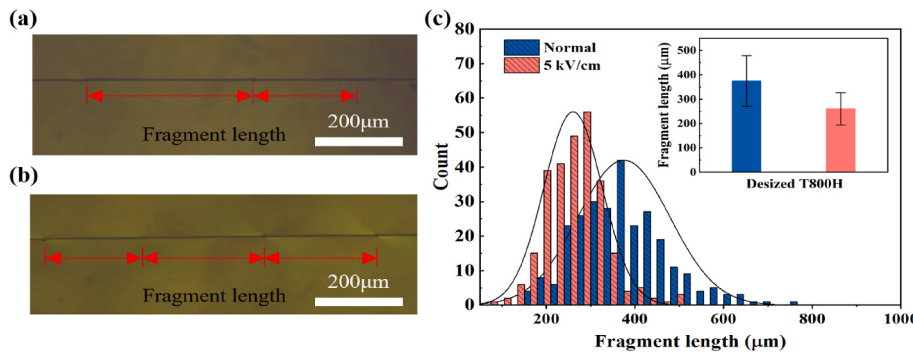


Fig. 6. Fringe patterns of single DT800H carbon fiber-epoxy composites prepared by (a) normal method and (b) electrically-assisted wetting method. (c) Comparison of distribution of critical fiber fragmentation length obtained in (a) and (b). The inset represents the mean values of critical lengths. The red arrows in (a–b) indicate the fragment lengths. (For interpretation of the references to colour in this figure legend, the reader is referred to the Web version of this article.)

interface than DT800H-EP composites owing to its smaller fractured length. In addition, for thorough verify the applicability of electrical stimulus induced enhancement, T300 carbon fiber was selected due to its similar surface morphology and different mechanical properties compared to T800-level carbon fiber (Fig. S9 and Table S1). As shown in Fig. S10, The average fragment length l_a of E-DT300-EP composites ($304.90 \pm 138.05 \mu\text{m}$) was 20.47% shorter than that of DT300-EP composites ($383.39 \pm 166.28 \mu\text{m}$). Hence, E-T300-Epoxy composites had a stronger interface than T300-Epoxy composites owing to its smaller fractured length. Overall, the interfacial mechanical properties of the composites suggested that electrowetting method could improve the interfacial adhesion strengths of carbon fiber-reinforced composites.

3.3. Computational analysis of electrowetting mechanism

To reveal the electrowetting mechanism and formation of mechanical interlock interface under an external electric field, infiltration of liquid epoxy resin into rough surfaces was conducted by finite element simulations. The simulations focused on epoxy flow behavior wetting the microstructured carbon fiber surface. Based on the experimental observation of wetting states in Figs. 2(a) and 3(b), the actuation of liquid epoxy was studied by applying an electric field as schematically illustrated in Fig. 7(a-b). Here, liquid epoxy droplets were placed on a simplified microstructured fiber surface. The carbon fiber and copper plate were used as electrodes. Since carbon fiber was fixed during the liquid epoxy resin filling process, the dynamic evolution of liquid epoxy

resin wetting process can be regarded as dynamic tracking of air-liquid interface under an external electric field. Hence, a two-phase flow model was used to describe the development of air-liquid interface morphology, consisting of Maxwell equation [53], Navier-Stokes equation [50] and Cahn-Hilliard equation [54]. In this case, it involves the coupling of the electric field and the flow field. Maxwell equation was used to describe the spatial electric field distribution of the liquid epoxy resin [53], and the Navier-Stokes equation was employed to describe the fluid (i.e. air and resin) [50]. On the other hand, the Cahn-Hilliard equation could be used to describe the properties of the fluid state and motion of the gas-liquid interface [54]. In the presence of an external electric field, the flow of liquid epoxy resin can be regarded as an incompressible Newtonian fluid, with a formulation (Eq. (2)) as [50]:

$$\begin{cases} \rho \frac{\partial \mathbf{u}}{\partial t} + \rho \mathbf{u} \cdot \nabla \mathbf{u} = -\nabla p + \eta \nabla^2 \mathbf{u} + \frac{1}{3} \eta \nabla (\nabla \cdot \mathbf{u}) + \mathbf{f}^e + \mathbf{F}_{st} + \rho \mathbf{g} \\ \frac{\partial (\rho \mathbf{u})}{\partial t} + \nabla \cdot (\rho \mathbf{u}) = 0 \end{cases} \quad (2)$$

where ρ is the density of the liquid/ $\text{kg}\cdot\text{m}^{-3}$ (composed of air and epoxy resin); \mathbf{u} is the flow rate of the liquid/ $\text{m}\cdot\text{s}^{-1}$ (composed of air and epoxy resin); p is the pressure of the liquid/Pa (composed of air and epoxy resin); η is the dynamic viscosity of the liquid coefficient/ $\text{Pa}\cdot\text{s}$; \mathbf{g} is the acceleration due to gravity/ $\text{m}\cdot\text{s}^{-2}$. The left term is the body-dependent derivative of fluid velocity with time, the first term on the right represents the effect of external atmospheric pressure, and the second and

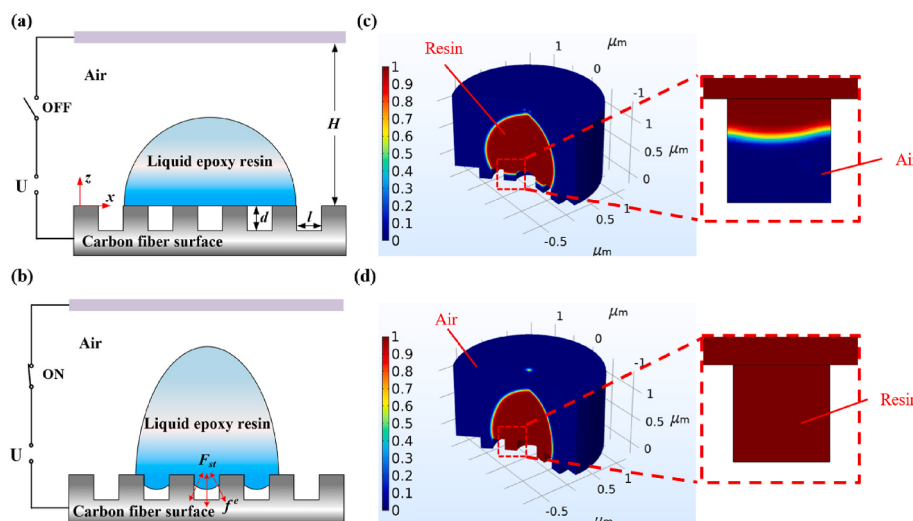


Fig. 7. (a–b) Schematic illustrations of two-phase flow models without/with the application of parallel electric field. (c–d) Finite element analysis of epoxy fluid behavior on structured substrate with and without application of electrical stimulus.

third terms represent the effect of viscous resistance. The fourth to sixth items represent the effects of electric field force, surface tension, and gravity, respectively. Because the fiber is round and the surface groove size is tiny, the influence of gravity is ignored. In the formula, the electric field force F^e is the Maxwell stress in the form of volume force suitable for the phase field model. The detailed description about the computational analysis has been depicted in the **Section S1** (Supporting information). The various parameters for the calculations are given in **Table S3**. This dynamic model was exploited to study the interface rheology in COMSOL MULTIPHYSICS software.

The steady-state rheological results of liquid resin on the rough surface without applied electric fields are summarized in **Fig. 7(c)**. The resin did not completely fill the cavities on the surface, consistent with the experimental results of **Fig. 2(a)**. The reason for this had to do with the surface tension F_{st} acting as a resistance to prevent the resin from flowing into the grooves. The interaction between fiber and matrix was limited and effect of mechanical interlock was not obvious, leading to the formation of weak interfaces in the composites. With the assistance of external electric field, the liquid epoxy could completely fill the microstructures, and wetting states changed from Cassie state to Wenzel state (**Fig. 7(d)**). The driving forces of the fluid generated by the electric field at the air-liquid interface highly depended on the electric field distribution. The electric field became mostly uniform inside the droplet when the liquid epoxy fully filled the microcavities (**Fig. S11**). Under the electric field, the Maxwell stress F^e generated by the electric field at the air-liquid interface acted as a force to drive the flow of liquid resin, confronting the resistance of surface tension F_{st} (**Fig. 7(b)**). The resistance also included viscous resistance of the fluid, which was not shown in **Fig. 7(b)**, but it was still considered in the simulation. For obtaining sufficient large Maxwell stress and completing the wetting transition, two-dimensional finite element simulations were performed to provide insights into the critical electric field intensity for controlling the wetting states transition. **Fig. S12** shows the dependence of wetting state and filling rate of liquid resin in an individual cavity on external voltage. It is found that the liquid gradually fills the cavity as the increase of external electric field intensity. Until the voltage reaches 68.50 V, the microcavity is completely filled and the transition from Cassie–Baxter state to Wenzel state is finished. When the voltage is higher than the threshold voltage V_c , and the wetting transition time decreases rapidly as the voltage increases. This is attributed to the fact that the driving force generated by the electric field is far greater than the combination of surface tension F_{st} and viscous resistance, and the microstructure is directly filled within a short period of time.

4. Conclusions

A simple and environmental-friendly electrically-assisted wetting method was successfully used to improve the interfacial strength between carbon fibers and polymer matrices. The method promoted the interfacial wetting and formation of mechanical interlocking, advantageous for full use of carbon fiber structure. Quantitative analyses of the effects of electrical stimulus on carbon fiber–epoxy interfacial strengths were conducted through microdroplet debonding and single fiber fragmentation tests. The results revealed maximum IFSS of carbon fiber–epoxy interface reaching up to 119.69 MPa, a value 81.02% higher than that of original fiber-based composites. The two-phase flow dynamics simulations showed the occurrence of substantial Maxwell stress at the air-liquid interface, acting as a driving force for the flow of liquid resin into surface grooves. This, in turn, resulted in a strong mechanical interlock interface. In sum, the electrically-assisted wetting method is used to enhance various interfaces formed by different carbon fibers and polymer matrices. The suggested approach for enhancing the carbon fiber–polymer interface looks promising for the optimal design of high-performance composites.

Authorship statement

Xiaoming Chen: Conceptualization, Investigation, Funding acquisition. Kaiqiang Wen: Methodology, Validation, Investigation. Jie Zhang: Conceptualization, Supervision, Funding acquisition. Jinyou Shao: Conceptualization, Resources, Visualization. Chunjiang Wang: Investigation. Siyi Cheng: Methodology, Validation. Shuo Wang: Investigation. Hechuan Ma: Investigation, Molecular Dynamic Simulation. Hongmiao Tian: Finite Element analysis. Xiangming Li: Investigation. All authors contributed to drafting of the manuscript. The manuscript is approved by all authors for publication.

Declaration of competing interest

The authors declare that they have no known competing financial interests or personal relationships that could have appeared to influence the work reported in this paper.

Acknowledgements

The authors gratefully acknowledge support from the National Natural Science Foundation of China (NSFC) (Grant Numbers: 52175544, 52172098), the National Key R&D Program of China (No. 2020YFB1711300). The authors also thank the instrument Analysis Center of Xi'an Jiaotong University for the SEM and XPS work.

Appendix A. Supplementary data

Supplementary data to this article can be found online at <https://doi.org/10.1016/j.compositesb.2022.109751>.

References

- [1] Unterweger C, Duchoslav J, Stifter D, Fürst C. Characterization of carbon fiber surfaces and their impact on the mechanical properties of short carbon fiber reinforced polypropylene composites. *Compos Sci Technol* 2015;108:41–7.
- [2] Zhao Z, Bai P, Guan R, Murugadoss V, Liu H, Wang X, et al. Microstructural evolution and mechanical strengthening mechanism of Mg-3Sn-1Mn-1La alloy after heat treatments. *Mater Sci Eng, A* 2018;734:200–9.
- [3] Yang L, Han P, Gu Z. Grafting of a novel hyperbranched polymer onto carbon fiber for interfacial enhancement of carbon fiber reinforced epoxy composites. *Mater Des* 2021;200:109456.
- [4] Mamalis D, Murray JJ, McClements J, Tsikritis D, Koutsos V, McCarthy ED, et al. Novel carbon-fibre powder-epoxy composites: interface phenomena and interlaminar fracture behaviour. *Compos B Eng* 2019;174:107012.
- [5] Arnold CL, Beggs KM, Eyckens DJ, Stojcevski F, Servinis L, Henderson LC. Enhancing interfacial shear strength via surface grafting of carbon fibers using the Kolbe decarboxylation reaction. *Compos Sci Technol* 2018;159:135–41.
- [6] Fu Y, Li H, Cao W. Enhancing the interfacial properties of high-modulus carbon fiber reinforced polymer matrix composites via electrochemical surface oxidation and grafting. *Compos Appl Sci Manuf* 2020;130:105719.
- [7] Yao T-T, Zhang X-F, Zhang W-S, Liu Y-T, Liu Q, Wu G-P. Controlled attachment of polycarbonate nanoparticles on carbon fibers for increased resin impregnation and interfacial adhesion in carbon fiber composites. *Compos B Eng* 2021;224:109218.
- [8] Qu C-B, Wu T, Huang G-W, Li N, Li M, Ma J-L, et al. Improving cryogenic mechanical properties of carbon fiber reinforced composites based on epoxy resin toughened by hydroxyl-terminated polyurethane. *Compos B Eng* 2021;210:108569.
- [9] Wu Q, Wan Q, Yang X, Wang F, Zhu J. Effects of chain length of polyether amine on interfacial adhesion of carbon fiber/epoxy composite in the absence or presence of polydopamine bridging platform. *Appl Surf Sci* 2021;547:149162.
- [10] Chen X, Zheng M, Park C, Ke C. Direct measurements of the mechanical strength of carbon nanotube-poly(methyl methacrylate) interfaces. *Small* 2013;9(19):3345–51.
- [11] Qiu B, Sun T, Li M, Chen Y, Zhou S, Liang M, et al. High micromechanical interlocking graphene oxide/carboxymethyl cellulose composite architectures for enhancing the interface adhesion between carbon fiber and epoxy. *Compos Appl Sci Manuf* 2020;139:106092.
- [12] Paiva MC, Bernardo CA, Nardin M. Mechanical, surface and interfacial characterisation of pitch and PAN-based carbon fibres. *Carbon* 2000;38(9):1323–37.
- [13] Liu L, Yan F, Li M, Zhang M, Xiao L, Shang L, et al. Improving interfacial properties of hierarchical reinforcement carbon fibers modified by graphene oxide with different bonding types. *Compos Appl Sci Manuf* 2018;107:616–25.

- [14] Chen X, Zhang L, Zheng M, Park C, Wang X, Ke C. Quantitative nanomechanical characterization of the van der Waals interfaces between carbon nanotubes and epoxy. *Carbon* 2015;82:214–28.
- [15] Bismarck A, Kumru M, Springer J, Simitzis J. Surface properties of PAN-based carbon fibers tuned by anodic oxidation in different alkaline electrolyte systems. *Appl Surf Sci* 1999;143(1–4):45–55.
- [16] Gulyás J, Földes E, Lázár A, Pukánszky B. Electrochemical oxidation of carbon fibres: surface chemistry and adhesion. *Compos Appl Sci Manuf* 2001;32(3–4): 353–60.
- [17] Lee W, Lee J, Reucroft P. XPS study of carbon fiber surfaces treated by thermal oxidation in a gas mixture of O₂/O₂₊ N₂). *Appl Surf Sci* 2001;171(1–2):136–42.
- [18] Zhang G, Sun S, Yang D, Dodelet J-P, Sacher E. The surface analytical characterization of carbon fibers functionalized by H₂SO₄/HNO₃ treatment. *Carbon* 2008;46(2):196–205.
- [19] Mujin S, Baorong H, Yisheng W, Ying T, Weiqu H, Youxian D. The surface of carbon fibres continuously treated by cold plasma. *Compos Sci Technol* 1989;34(4):353–64.
- [20] Liang Y, Li X, Semitekolos D, Charitidis CA, Dong H. Enhanced properties of PAN-derived carbon fibres and resulting composites by active screen plasma surface functionalization. *Plasma Process Polym* 2020:e1900252.
- [21] Hung K-B, Li J, Fan Q, Chen Z-H. The enhancement of carbon fiber modified with electropolymer coating to the mechanical properties of epoxy resin composites. *Compos Appl Sci Manuf* 2008;39(7):1133–40.
- [22] Sun T, Li M, Zhou S, Liang M, Chen Y, Zou H. Multi-scale structure construction of carbon fiber surface by electrophoretic deposition and electropolymerization to enhance the interfacial strength of epoxy resin composites. *Appl Surf Sci* 2020;499: 143929.
- [23] Vautard F, Ozcan S, Paulauskas F, Spruiell JE, Meyer H, Lance MJ. Influence of the carbon fiber surface microstructure on the surface chemistry generated by a thermo-chemical surface treatment. *Appl Surf Sci* 2012;261:473–80.
- [24] Bekyarova E, Thostenson E, Yu A, Kim H, Gao J, Tang J, et al. Multiscale carbon nanotube–carbon fiber reinforcement for advanced epoxy composites. *Langmuir* 2007;23(7):3970–4.
- [25] Chen Q, Peng Q, Zhao X, Sun H, Wang S, Zhu Y, et al. Grafting carbon nanotubes densely on carbon fibers by poly (propylene imine) for interfacial enhancement of carbon fiber composites. *Carbon* 2020;158:704–10.
- [26] Zhang J, Zhuang R, Liu J, Mäder E, Heinrich G, Gao S. Functional interphases with multi-walled carbon nanotubes in glass fibre/epoxy composites. *Carbon* 2010;48(8):2273–81.
- [27] Cheng C, Zhang M, Wang S, Li Y, Feng H, Bu D, et al. Improving interfacial properties and thermal conductivity of carbon fiber/epoxy composites via the solvent-free GO@Fe₃O₄ nanofluid modified water-based sizing agent. *Compos Sci Technol* 2021;209:108788.
- [28] Han SH, Oh HJ, Kim SS. Evaluation of fiber surface treatment on the interfacial behavior of carbon fiber-reinforced polypropylene composites. *Compos B Eng* 2014;60:98–105.
- [29] Qiu B, Sun T, Yuan M, Zhang H, Chen Y, Zhou S, et al. Effect of different lateral dimension graphene oxide sheets on the interface of carbon fiber reinforced polymer composites. *Compos Sci Technol* 2021;213:108939.
- [30] Liu L, Jia C, He J, Zhao F, Fan D, Xing L, et al. Interfacial characterization, control and modification of carbon fiber reinforced polymer composites. *Compos Sci Technol* 2015;121:56–72.
- [31] Chen L, Wei F, Liu L, Cheng W, Hu Z, Wu G, et al. Grafting of silane and graphene oxide onto PBO fibers: multifunctional interphase for fiber/polymer matrix composites with simultaneously improved interfacial and atomic oxygen resistant properties. *Compos Sci Technol* 2015;106:32–8.
- [32] Zhang S-j, Wang R-m, Liao Y-q. A comparative study of two kinds of T800 carbon fibers produced by different spinning methods for the production of filament-wound pressure vessels. *N Carbon Mater* 2019;34(6):578–86.
- [33] Fitzer E, Weiss R. Effect of surface treatment and sizing of C-fibres on the mechanical properties of CFR thermosetting and thermoplastic polymers. *Carbon* 1987;25(4):455–67.
- [34] Xu P, Yu Y, Liu D, He M, Li G, Yang X. Enhanced interfacial and mechanical properties of high-modulus carbon fiber composites: establishing modulus intermediate layer between fiber and matrix based on tailored-modulus epoxy. *Compos Sci Technol* 2018;163:26–33.
- [35] Gao S-L, Mäder E, Zhadarov SF. Carbon fibers and composites with epoxy resins: topography, fractography and interphases. *Carbon* 2004;42(3):515–29.
- [36] Bormashenko E, Pogreb R, Whyman G, Bormashenko Y, Erlich M. Vibration-induced Cassie-Wenzel wetting transition on rough surfaces. *Appl Phys Lett* 2007; 90(20):201917.
- [37] Bormashenko E, Pogreb R, Balter S, Aurbach D. Electrically controlled membranes exploiting Cassie-Wenzel wetting transitions. *Sci Rep* 2013;3:3028.
- [38] Tabassian R, Oh J-H, Kim S, Kim D, Ryu S, Cho S-M, et al. Graphene-coated meshes for electroactive flow control devices utilizing two antagonistic functions of repellency and permeability. *Nat Commun* 2016;7(1):1–9.
- [39] Kasahara S, Koyanagi J, Mori K, Yabe M. Evaluation of interface properties of carbon fiber/resin using the full atomistic model considering the electric charge state. *Adv Compos Mater* 2020;30(2):164–75.
- [40] Yuan X, Zhu B, Cai X, Qiao K, Zhao S, Zhang M, et al. Micro-configuration controlled interfacial adhesion by grafting graphene oxide onto carbon fibers. *Compos Appl Sci Manuf* 2018;111:83–93.
- [41] Coleman JN, Khan U, Blau WJ, Gun'ko YK. Small but strong: a review of the mechanical properties of carbon nanotube–polymer composites. *Carbon* 2006;44(9):1624–52.
- [42] Koyanagi J, Ogihara S, Nakatani H, Okabe T, Yoneyama S. Mechanical properties of fiber/matrix interface in polymer matrix composites. *Adv Compos Mater* 2014; 23(5–6):551–70.
- [43] Zhang T, Cheng Q, Xu Z, Jiang B, Wang C, Huang Y. Improved interfacial property of carbon fiber composites with carbon nanotube and graphene oxide as multi-scale synergistic reinforcements. *Compos Appl Sci Manuf* 2019;125:105573.
- [44] Wu Q, Zhao R, Xi T, Yang X, Zhu J. Comparative study on effects of epoxy sizing involving ZrO₂ and GO on interfacial shear strength of carbon fiber/epoxy composites through one and two steps dipping routes. *Compos Appl Sci Manuf* 2020;134:105909.
- [45] Yan F, Liu L, Li K, Jin L, Zhang M, Liu Y, et al. A novel π bridging method to graft graphene oxide onto carbon fiber for interfacial enhancement of epoxy composites. *Compos Sci Technol* 2021;201:108489.
- [46] Wu Q, Yang X, Wan Q, Zhao R, He J, Zhu J. Layer-by-layer assembled nacre-like polyether amine/GO hierarchical structure on carbon fiber surface toward composites with excellent interfacial strength and toughness. *Compos Sci Technol* 2020;198:108296.
- [47] Dong J, He J, Jia C, Song Y, He Z, Wei H, et al. Growth of carbon black onto continuous carbon fiber to produce composites with improved mechanical and interfacial properties: a step closer to industrial production. *Compos Sci Technol* 2019;173:83–9.
- [48] Xu N, Lu C, Zheng T, Qiu S, Liu Y, Zhang D, et al. Enhanced mechanical properties of carbon fibre/epoxy composites via in situ coating-carbonisation of micron-sized sucrose particles on the fibre surface. *Mater Des* 2021;200:109458.
- [49] Xu D, Liu B, Zhang G, Long S, Wang X, Yang JJHPP. 4. Effect of air plasma treatment on interfacial shear strength of carbon fiber-reinforced polyphenylene sulfide, vol. 28; 2016. p. 411–24.
- [50] Tian H, Shao J, Ding Y, Li X, Liu H. Numerical characterization of electrohydrodynamic micro- or nanopatterning processes based on a phase-field formulation of liquid dielectrophoresis. *Langmuir* 2013;29(15):4703–14.
- [51] Kim I-S, Ko P-J, Cho M-Y, Lee Y-S, Sohn H, Park C, et al. Fabrication of high-quality alumina coating through novel, dual-particle aerosol deposition. *Ceram Int* 2020; 46(15):23686–94.
- [52] Wang Z, Zhao Y-P. Wetting and electrowetting on corrugated substrates. *Phys Fluids* 2017;29(6):067101.
- [53] Wheeler JA, Feynman RP. Classical electrodynamics in terms of direct interparticle action. *Rev Mod Phys* 1949;21(3):425.
- [54] Cahn JW, Hilliard JE. Free energy of a nonuniform system. I. Interfacial free energy. *J Chem Phys* 1958;28(2):258–67.

Supplementary Material

Enhancing Mechanical Strength of Carbon Fiber-Epoxy Interface through Electrowetting of Fiber Surface

Xiaoming Chen,^{1,†} Kaiqiang Wen,^{1,†} Chunjiang Wang,¹ Siyi Cheng,¹ Shuo Wang,¹ Hechuan Ma,¹ Hongmiao Tian,¹ Jie Zhang,^{2,*} Xiangming Li,¹ Jinyou Shao^{1,*}

¹Micro- and Nanotechnology Research Center, State Key Laboratory for Manufacturing Systems Engineering, Xi'an Jiaotong University, Xi'an, Shaanxi 710049, China

²Electronic Materials Research Laboratory, Key Laboratory of the Ministry of Education & International Center for Dielectric Research, School of Electronic Science and Engineering, Xi'an Jiaotong University, Xi'an 710049, China

[†]These authors contributed equally to this paper.

*To whom correspondence should be addressed. jzhang12@xjtu.edu.cn (J. Zhang) and jyshao@xjtu.edu.cn (J. Shao)

1. Computational analysis

The generalized modeling of the microstructure electrowetting filling process involves five field problems governed by the following [1]:

(1) The Cahn–Hilliard equation for a dual-phase diffusion governs the mass conservation and is represented in terms of the phase-field function, φ , as follows (Eq. (S1)) [2]:

$$\frac{\partial \varphi}{\partial t} + \nabla \cdot (\mathbf{u}\varphi) = \nabla \cdot (\mu \nabla G) \quad (1)$$

where ∇ stands for a gradient operator; \mathbf{u} is the flow rate of the liquid and gas/ m·s⁻¹; μ is the fluid mobility/ s·Kg⁻¹; G is the chemical potential /J. The second term on the left-hand side of the equation represents the convection flux and the righthand term the diffusion flux.

The chemical potential G is the partial differential of the overall free energy of the system with respect to the phase function φ . Thus, the trend of the movement of the phase function φ can be obtained. According to the phase function φ and the chemical potential G , the surface tension F_{st} at the gas-liquid interface can be deduced as (Eq. (S2))[3-5]:

$$F_{st} = G \nabla \varphi \quad (2)$$

The expression form of volume force of surface tension is similar to that of electric field force. It is concentrated at the gas-liquid interface, which tends to 0 at a position away from the gas-liquid interface. This can be attributed to the distribution of the phase function φ in the spatial position.

(2) The Navier–Stokes hydrodynamic equations of momentum and mass conservation for the movement of the fluid are written as Eq. (2).

(3) Gauss's law for the electric field is represented in the following Maxwell equation (Eq. (S3))

$$\nabla \cdot (\epsilon \mathbf{E}) = \rho^e \quad \epsilon = \epsilon_0 \epsilon_r \quad (3)$$

where ρ^e is the spatial density for free charges in a leaky dielectric liquid, ϵ_0 is the vacuum permittivity, ϵ_r is the relative permittivity of the problem domain (air and polymer), and \mathbf{E} is the electric field. Here the air and polymer involved in microstructure electrowetting filling process are both dielectric (perfect or leaky), and the magnetic effect can be neglected; i.e., the electric field is considered to be irrotational. With the availability of the electric field, the electrodynamic pressure f^e in the Navier–Stokes hydrodynamic equations (Eq. (2)) can be determined by the following relationship (Eq. (S4)) [6]

$$f^e = \rho_e \mathbf{E} - \frac{1}{2} E^2 \nabla \epsilon \quad (4)$$

The first and second terms on the right-hand side are the contribution from the Coulomb force and dielectric force, respectively.

(4) The charge conservation law governing the spatial charge motion is essential to determine the movement of the free space charges, especially on the air-polymer interface, is expressed by [7] (Eq. (S5))

$$\frac{\partial \rho^e}{\partial t} + \mathbf{u} \cdot \nabla \rho^e = -\nabla \cdot (\sigma \mathbf{E}) \quad (5)$$

where σ is the electrical conductivity for the leaky dielectric polymer. The second term on the left-hand side of Eq. (S5) represents a transport of the free charges by convection, and the term on the right-hand side stands for the transport by electromigration.

(5) In the macroscopic state, the dynamic viscosity coefficient of polymer fluid is constant and has limited effects on spatial position. However, at the micro-nano scale, the dynamic viscosity coefficient η is not constant due to the physical adhesion of polymer molecules on the solid wall. It is related to the force between fluid molecules and the position in space. The viscosity expression in Eringen-Okada form[8] (Eq. (S6)):

$$\eta = \eta_b [1 + \zeta (\tau / D^2)] \quad (6)$$

where η is the dynamic viscosity coefficient of the polymer at the micro-nano scale/Pa·s; η_b is the macroscopic bulk viscosity coefficient of the polymer/Pa·s; ζ is the material property parameter/dimensionless; τ is the radius of gyration of the resin molecule/m; D is the distance from the solid wall/m.

The polymer's evolving deformation for the microstructure electrowetting filling process can be obtained numerically by a simultaneous solving of Eq. (S1) (2) (S3) (S5) and (S6). For a dielectric polymer (as a special case) the electrical conductivity σ and the free charge ρ^e can be set to zero so that Eq. (S5) is eliminated automatically. In our case, it is assumed that the temperature has slight effect. Therefore, the temperature is regarded as a constant parameter in the simulation calculation, so the fluid viscosity, surface tension and other parameters are unchanged.

In consequence, a numerical analysis is performed to study the microstructure electrowetting filling process. The iteration of this coupled problems is carried out by the finite element method in COMSOL MULTIPHYSICS software, in which the governing equations described in the preceding are defined explicitly and symbolically

and then automatically solved by the Galerkin approach. Once the phase-field function φ is obtained, the moving air-liquid interface can be easily identified by tracing a zero-value contour of the phase-field function or by simply color-mapping the phase-field function, providing a visualization of the polymer's deformation step by step.

Table S1: Mechanical parameters of carbon fiber: T800H, T800S and T300.

Carbon fiber	Diameter (μm)	Tensile Strength (GPa)	Tensile modulus (GPa)
T800H	4.8 \pm 0.3	5.66 \pm 0.66	289 \pm 33
T800S	5.1 \pm 0.2	6.07 \pm 0.91	293 \pm 42
T300	7.2 \pm 0.4	3.47 \pm 0.30	225 \pm 16

Table S2: Surface element of the epoxy resin coated carbon fiber with and without application of electrical stimulus.

Samples	Element composition (%)			
	C1s	O1s	N1s	O/C
T800H-EP	68.98	28.53	2.49	41.35
E-T800H-EP	69.48	28.66	1.86	41.25
DT800H-EP	69.79	27.88	2.33	39.95
E-DT800H-EP	70.05	27.56	2.39	39.34

Table S3: Various parameters used in computational analysis.

Parameters	Value
Relative permittivity of polymer	7
Relative permittivity of air	1
Viscosity of polymer	0.8 Pa·s
Surface tension coefficient of the air–polymer interface	0.03 N/m
Mass density of polymer	980 kg/m ³
Initial contact angle	120°

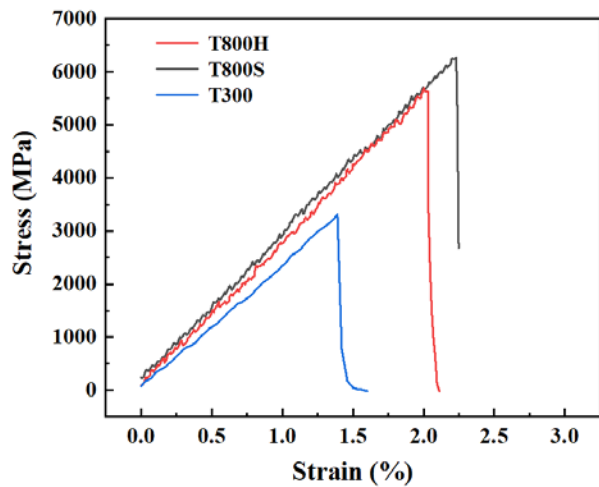


Figure S1: Typical stress-strain curves for T800S, T800H and T300 single carbon fibers.

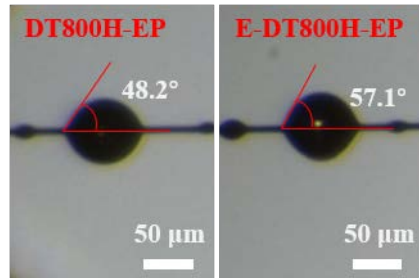


Figure S2: Contact angle of resin droplets on single fiber with and without application of electrical stimulus.

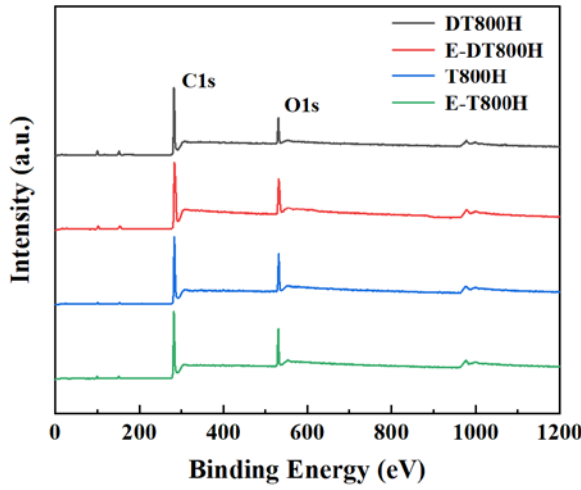


Figure S3: The full-scan XPS spectra of T800H, E-T800H, DT800H and E-DT800H.

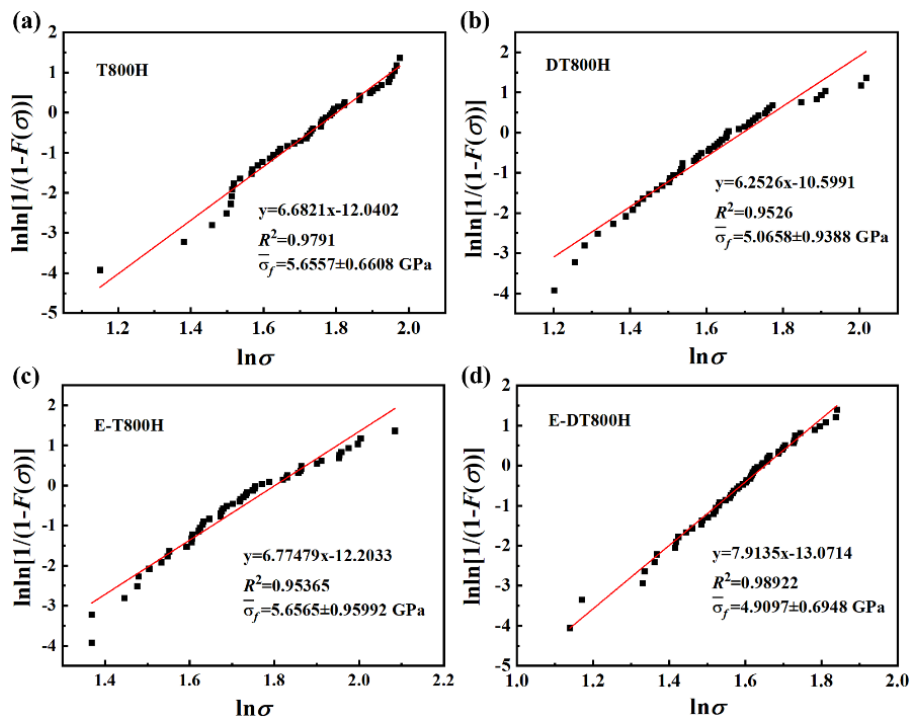


Figure S4: The Weibull distribution of single fiber tensile strength (a) T800H; (b) DT800H; (c) E-T800H; (d) E-DT800H.

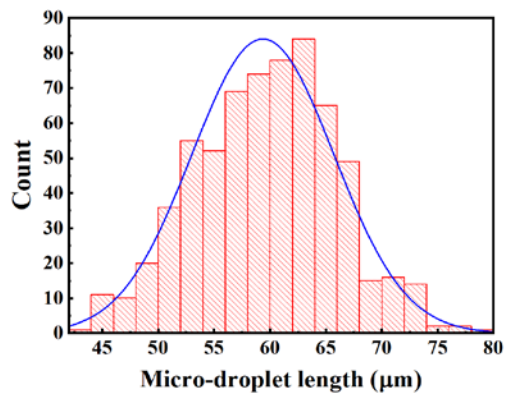


Figure S5: The Normal distribution of micro-droplet length.

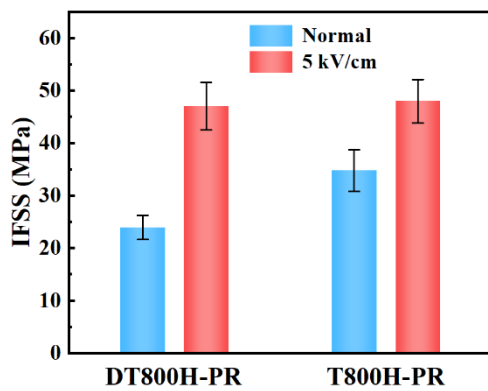


Figure S6: The influence of electric stimulus on IFSS of T800H-PR interfaces.

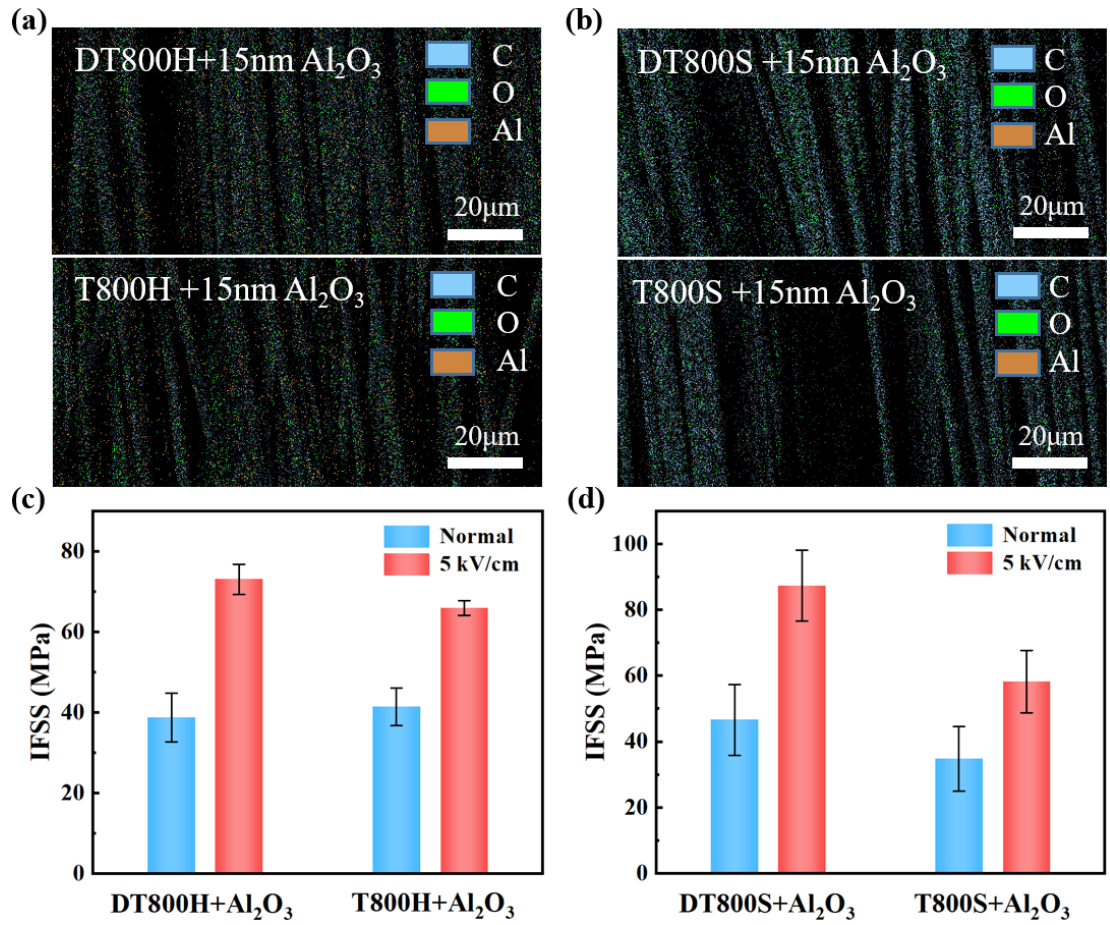


Figure S7: Characterized surface element content of carbon fibers by EDS: (a)T800H; (b)T800S. IFSS of composites composed of single carbon fibers coated with a 15 nm Al₂O₃ layer: (c) T800H; (d) T800S.

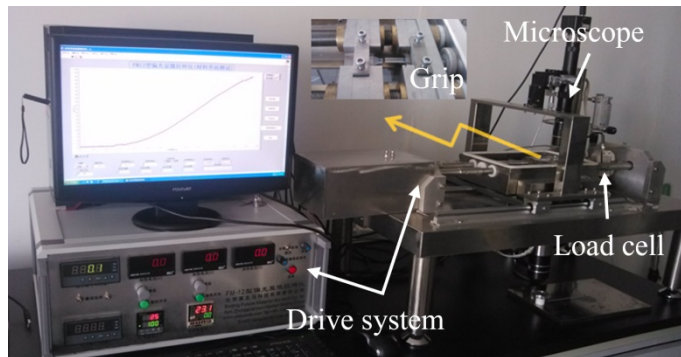


Figure S8: Experimental setup for single fiber fragmentation test

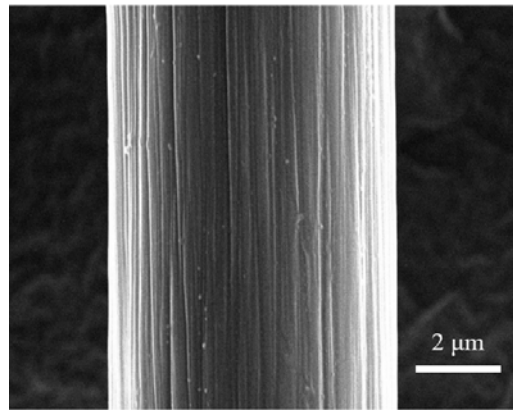


Figure S9: Surface morphology of T300 by SEM.

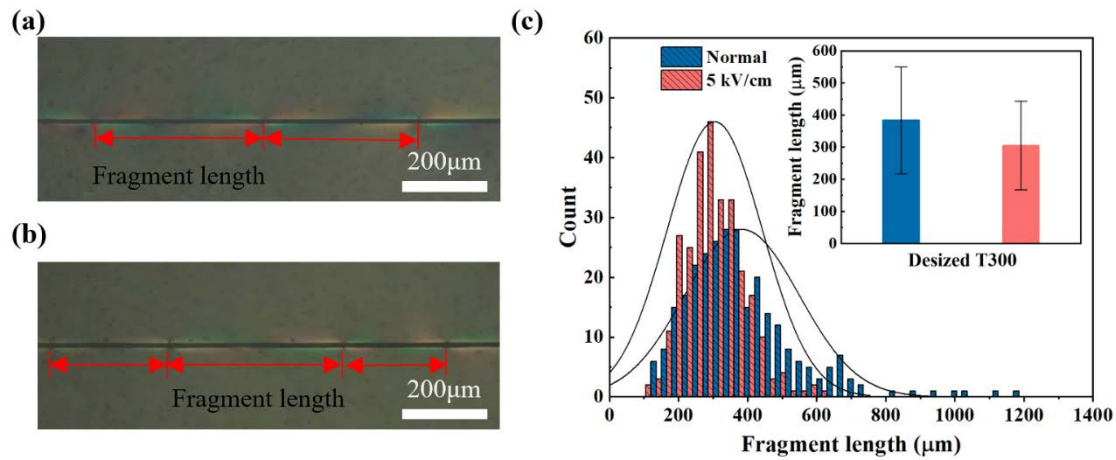


Figure S10: Fringe patterns of single DT300 carbon fiber-epoxy composites prepared by (a) normal method and (b) electrically assisted-wetting method. (c) Comparison of distribution of critical fiber fragmentation length obtained in (a) and (b). The inset represents the mean values of critical lengths. The red arrows in (a-b) indicate the fragment lengths.

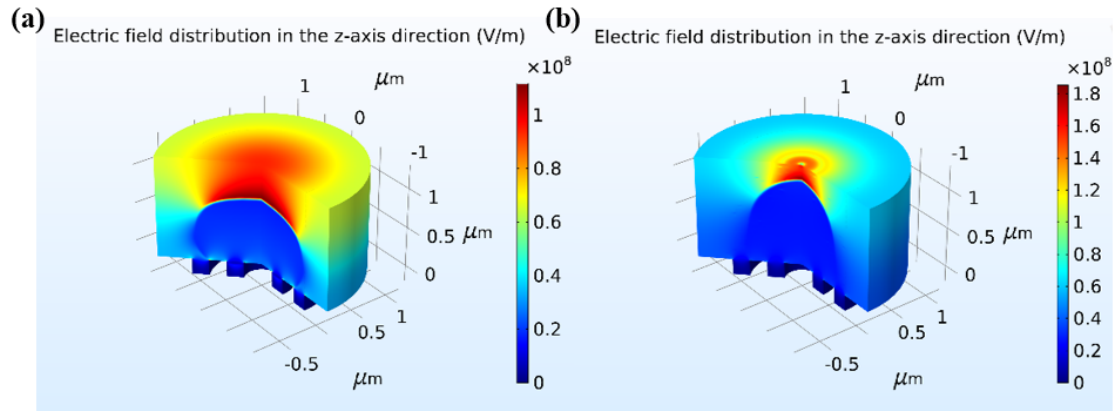


Figure S11: Electric field distribution (a) Initial state; (b) Final state.

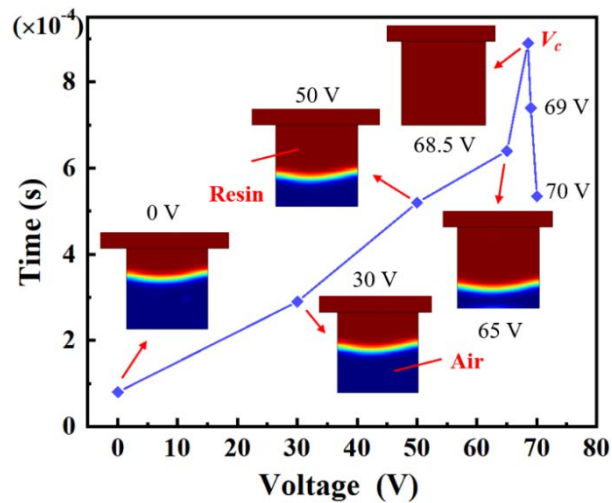


Figure S12: The dependence of the time to reach steady state on electric field intensity.

References

- [1] Tian H, Wang C, Shao J, Ding Y, Li X. Electrohydrodynamic pressure enhanced by free space charge for electrically induced structure formation with high aspect ratio. *Langmuir*. 2014;30(42):12654-63.
- [2] Cahn JW, Hilliard JE. Free energy of a nonuniform system. III. Nucleation in a two - component incompressible fluid. *The Journal of chemical physics*. 1959;31(3):688-99.
- [3] Yue P, Feng JJ, Liu C, Shen JJJoFM. A diffuse-interface method for simulating two-phase flows of complex fluids. 2004;515:293.
- [4] Lowengrub J, Truskinovsky LJPotRSoLSAM, Physical, Sciences E. Quasi-incompressible Cahn–Hilliard fluids and topological transitions. 1998;454(1978):2617-54.
- [5] Tian H, Shao J, Ding Y, Li X, Li XJE. Numerical studies of electrically induced pattern formation by coupling liquid dielectrophoresis and two - phase flow. 2011;32(17):2245-52.
- [6] Zeng J, Korsmeyer T. Principles of droplet electrohydrodynamics for lab-on-a-chip. *Lab Chip*. 2004;4(4):265-77.
- [7] Yang Q, Li BQ, Ding Y. 3D phase field modeling of electrohydrodynamic multiphase flows. *International Journal of Multiphase Flow*. 2013;57:1-9.
- [8] Yao D, Kim B. Simulation of the filling process in micro channels for polymeric materials. *Journal of micromechanics and microengineering*. 2002;12(5):604.